



Geophysical Research Letters[®]



RESEARCH LETTER

10.1029/2022GL098477

Subsidence in Coastal Cities Throughout the World Observed by InSAR

Pei-Chin Wu¹ , Meng (Matt) Wei¹ , and Steven D'Hondt¹

¹Graduate School of Oceanography, University of Rhode Island, Kingston, RI, USA

Key Points:

- We measured the subsidence rate for 99 coastal cities around the world between 2015 and 2020 using the PS Interferometric Synthetic Aperture Radar method and Sentinel-1 data
- In most cities, part of the land is subsiding faster than sea level is rising and will be challenged by flooding sooner than expected
- Coastal nations must institute continuous monitoring and policy interventions to reduce subsidence rates and minimize their consequences

Supporting Information:

Supporting Information may be found in the online version of this article.

Correspondence to:

M. (M.) Wei,
matt-wei@uri.edu

Citation:

Wu, P.-C., Wei, M. (M.), & D'Hondt, S. (2022). Subsidence in coastal cities throughout the world observed by InSAR. *Geophysical Research Letters*, 49, e2022GL098477. <https://doi.org/10.1029/2022GL098477>

Received 28 FEB 2022
Accepted 8 MAR 2022

Abstract We measured subsidence rates in 99 coastal cities around the world between 2015 and 2020 using the PS Interferometric Synthetic Aperture Radar method and Sentinel-1 data. In most cities, part of the land is subsiding faster than sea level is rising. If subsidence continues at present rates, these cities will be challenged by flooding much sooner than projected by sea level rise models. The most rapid subsidence is occurring in South, Southeast, and East Asia. However, rapid subsidence is also happening in North America, Europe, Africa, and Australia. Human activity—primarily groundwater extraction—is likely the main cause of this subsidence. Expanded monitoring and policy interventions are required to reduce subsidence rates and minimize their consequences.

Plain Language Summary Satellite data indicate that land is subsiding faster than sea level is rising in many coastal cities throughout the world. If subsidence continues at recent rates, these cities will be challenged by flooding much sooner than projected by sea level rise models. We measured subsidence rates in 99 coastal cities around the world between 2015 and 2020 using satellite data. Subsidence rates are highly variable within cities and from city to city. The most rapid subsidence is occurring in South, Southeast, and East Asia. However, rapid subsidence is also happening in North America, Europe, Africa, and Australia. Human activity—primarily groundwater extraction—is likely the main cause of this subsidence. Expanded monitoring and policy interventions are required to reduce subsidence rates and minimize their consequences.

1. Introduction

In many coastal cities, land is subsiding faster than sea level is rising (Cao et al., 2021; Erkens et al., 2015; Nicholls et al., 2021). If subsidence continues at recent rates, these cities will be challenged by severe flood events much sooner than projected by sea level rise models (Kulp & Strauss, 2019; Shirzaei & Burgmann, 2018). Subsidence rate is highly variable in space and time owing to multiple processes (Esteban et al., 2020; Shirzaei et al., 2021). Processes that affect coastal vertical motions include Glacial Isostatic Adjustment (GIA) and non-GIA components, with the latter including tectonic movement (Dokka, 2006), sediment settling, and aquifer-system compaction (Hamlington et al., 2020). Glacial Isostatic Adjustment occurs mostly in high-latitude regions with a slow and steady rate (a few mm/yr). Tectonic movement affects areas with active faults in both steady and transient manner (Smith-Konter et al., 2014). Although sediment and aquifer compaction can happen naturally, they can be greatly accelerated by human activities, including ground water extraction related to rapid urbanization and population growth (Collados-Lara et al., 2020; Erkens et al., 2015; Ward et al., 2011), oil and gas production (Fielding et al., 1998; Métois et al., 2020), and new building loads (Ciampalini et al., 2019; Dixon et al., 2006; Galloway et al., 1999; He et al., 2021). The dominant processes and their contributions to coastal subsidence vary from place to place, making it a challenging task to understand and address coastal subsidence.

Modern tools with high spatial and temporal coverage have been used to monitor coastal subsidence at a regional level with huge success (Chaussard et al., 2013; Hung et al., 2018; Karegar et al., 2017; Sato et al., 2006; Shirzaei et al., 2021; Teatini et al., 2005). Permanent Global Navigation Satellite System (GNSS) stations can provide accurate measurements of coastal subsidence (mm/yr) but are limited in their spatial coverage and spatial resolution. Interferometric Synthetic Aperture Radar (InSAR) can provide much greater spatial resolution with reasonable accuracy (a few mm/yr). In places with a dense GNSS network, such as California, it has been proven that combining InSAR and GNSS can achieve regional coverage of coastal subsidence at both high accuracy and high spatial coverage (Blackwell et al., 2020; Farolfi et al., 2019; Hammond et al., 2018; Hu et al., 2019; Morishita, 2021; Yalvac, 2020). In places where GNSS stations are sparse or absent, InSAR remains the best tool to monitor coastal subsidence. Optical leveling and LiDAR are also used but suffer major limitations. Optical

© 2022. The Authors.

This is an open access article under the terms of the [Creative Commons Attribution License](https://creativecommons.org/licenses/by/4.0/), which permits use, distribution and reproduction in any medium, provided the original work is properly cited.

leveling is labor intensive and has limited spatial coverage. LiDAR can be expensive to process and lacks global coverage.

On a global scale, knowledge of coastal subsidence status is spatially and temporally limited. Herrera-Garcia et al. (2021) conducted a comprehensive literature search, finding that land subsidence due to groundwater depletion occurred at 200 locations in 34 countries during the past century. Some of their 200 locations are coastal. They did not consider subsidence magnitude and rate because much of the literature lacks this information. Shirzaei et al. (2021) created a global coastal subsidence map using GNSS data. Although the global extent of their coverage is impressive, their spatial resolution is limited to the exact locations of GNSS stations. Due to this spatial limitation, the GNSS results set a lower bound on the number of cities experiencing active coastal subsidence. Due to the same limitation, they generally do not record the full rate and extent of subsidence in individual cities. To fill these gaps, we measured subsidence rates in 99 cities around the world between 2015 and 2020 using the Persistent Scatterer InSAR (PS-InSAR) method and Sentinel-1 data.

2. Data and Methods

We used SAR data between October 2014 and January 2021 from the C-band Sentinel-1 A/B, which was commissioned and funded by the European Commission and the European Space Agency (ESA). For each city, we processed one satellite image every 2 months and used a total of six images per year to establish the long-term time series of the deformation rate. We searched for and downloaded the SAR data from the online portal of the Alaska Satellite Facility. Depending on the data quality and availability, the time range of data varies between cities and the average is 5.3 years (Table S1).

We used software SNAP (version 8.0.3) to make interferograms and software StaMPS (version 4.0b) to extract time series of ground displacements from PS-InSAR.

SNAP was developed by ESA for processing Sentinel-1 SAR data. The software registers images and calculated interferograms by differencing the phase of two repeating SAR images. A 30-m resolution Shuttle Radar Topography Mission (SRTM) digital elevation map (DEM) was used to remove the topographic effect. We chose the SAR image in the midpoint of the time range as the master. All other images were co-registered with the master. Then SNAP exports the co-registered stack, interferograms, and DEM data within a folder structure accepted by StaMPS.

StaMPS was developed by Hooper et al. (2004) to calculate PS-InSAR time series. The software identifies coherent pixels, selects PS points, estimates spatially correlated look-angle error and extracts the deformation relative to the master image for these pixels. We used default values for all parameters. For areas with significant elevation change across the InSAR image, we applied a linear elevation noise correction using the Toolbox for Reducing Atmospheric InSAR Noise (TRAIN), developed by Bekaert et al. (2015).

We attempted to use GNSS data from the Nevada Geodetic Lab database to register the InSAR data. For cities with GNSS data overlap with our InSAR data in space and time, we used one GNSS station to register the deformation rate map calculated by StaMPS. For cities that do not have open GNSS data, we chose a small area outside of the urban area as reference. This reference area is circular with a radius of 5 km. It is typically an elevated region away from the shore. Details can be found in Table S1.

In short, we plotted the time series of deformation calculated by StaMPS and referenced by either GNSS data or stable area and calculated the average deformation rate at specific areas in different cities. To speed up processing, we only used one track of SAR images for each city and assumed the deformation to be mainly in the vertical direction. Although there is some horizontal movement toward centers of water, oil, or gas extraction, the assumption that most deformation is vertical is valid in most cases. The primary exceptions to this assumption are locations of major transform faults, such as Los Angeles (California), which are excluded from this study.

3. Results and Discussion

3.1. Global Patterns

These satellite-based results indicate that subsidence is common in cities through the world. Figure 1 summarizes the global pattern for 99 cities in two ways. Figure 1a shows the maximum subsidence rate (line-of-sight

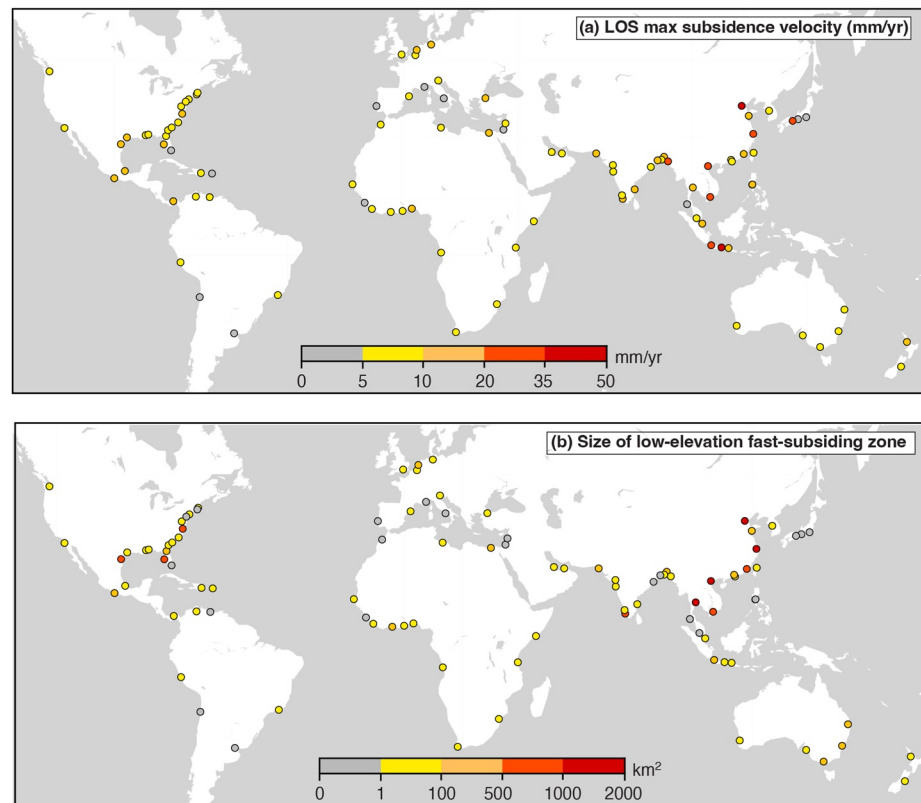


Figure 1. (a) The maximum subsidence rate (line-of-sight [LOS] displacement) in 99 cities around the world using Sentinel-1 A/B data between 2015 and 2020. (b) Estimated area with elevation less than 10 m above sea level and subsidence faster than 2 mm/yr LOS in the Interferometric Synthetic Aperture Radar time series map within the city boundary. Subsidence of 2 mm/yr LOS is at the lower end of the current global sea level rise rate (2.6 mm/yr for past two decades by Nicholls et al. (2021); 2.1 ± 0.9 mm/yr for 1971–2010 and 3.0 ± 1.9 mm/yr for 1993–2010 by Palmer et al. (2021)).

[LOS] displacement) found in each city. Figure 1b shows the estimated total area with an elevation less than 10 m from sea level that is subsiding faster than 2 mm/yr LOS within each city boundary. Details can be found in Table S1. The 2 mm/yr LOS rate indicates 2.2–2.6 mm/yr vertical deformation (depending on the location of the pixel within the image and assuming no horizontal deformation). This subsidence rate approximates recent estimates of global sea level rise rate (2.6 mm/yr for past two decades by Nicholls et al. (2021); 2.1 ± 0.9 mm/yr for 1971–2010 and 3.0 ± 1.9 mm/yr for 1993–2010 by Palmer et al. (2021)).

In most cities, part of the city is sinking faster than 2 mm/yr LOS. In 33 of the 99 cities, part of the city is sinking equal to or more than 10 mm/yr LOS— $\geq 5x$ faster than global mean sea level is rising. These cities with fast sinking regions are located throughout the world, including in Europe, North America, Africa, and Australia. The cities where subsidence has been the fastest (over 20 mm/yr LOS) from 2015 to 2020 are in South, Southeast, and East Asia. The highest subsidence rates appear in Tianjin, Semarang, and Jakarta, where maximum rates exceed 30 mm/yr LOS—dwarfing global mean sea level rise by almost 15x.

To estimate the areas where subsidence has the most immediate potential for increased risk of future flooding, we estimated the total area within each urban area that is elevated less than 10 m from sea level and subsiding faster than 2 mm/yr LOS (Figure 1b). The 2 mm/yr threshold is comparable to the rate of global mean sea level rise. We selected the 10-m elevation cutoff because flooding reached 9.1 m during the 2005 hurricane Katrina (Fritz et al., 2007) and the storm surge will continue to increase as sea level rises (Garner et al., 2017). We used the SRTM DEM to identify low-elevation areas. To define urban areas, we used either a city boundary found online or an urban boundary that we digitized. To estimate the area of the fast-sinking low-elevation portion of each city, we calculated the total area in the city that has an elevation less than 10 m and calculated the percentage of PS points in that low-elevation area that is subsiding faster than 2 mm/yr. Then, we multiplied the total low-elevation

area by this percentage to get the potential size of the low-elevation area subsiding faster than 2 mm/yr. This step is necessary because some portions of the low-elevation areas have no PS points. Based on this calculation, four cities have more than 1000 km² of low-elevation area subsiding faster than sea level is rising (2 mm/yr LOS). Eighteen cities have between 100 and 1000 km² and 24 have between 10 and 100 km² of low-elevation area subsiding faster than 2 mm/yr. For each city, we also estimated the area elevated less than 5 m from sea level that is sinking faster than 2 mm/yr (Table S1). In general, cities with more area for the 10 m case have also more area for the 5 m case (Figure S1 in Supporting Information S1). On average, the estimated low-elevation, fast-subsidence area for 5 m is 63% of that for 10 m (Figure S1 in Supporting Information S1).

Subsidence of a few mm/yr is close to the uncertainty of InSAR time series for about 5 years of data (Osmanoglu et al., 2016). Consequently, InSAR-based interpretations of subsidence rates slower than 2 mm/yr (the approximate rate of sea level rise) require independent verification (e.g., with GNSS data) or longer time series. To demonstrate the validity of our method, we compared our results with additional GNSS data at Melbourne (Australia). Our InSAR results are broadly consistent with the additional GNSS results (Figure S2 in Supporting Information S1). In many cities, however, GNSS stations are not present in the areas indicated by InSAR to be subsiding. This issue is illustrated by results for Istanbul (Turkey) and Lagos (Nigeria) (Figure 2). Only three GNSS stations are available for Istanbul. There are no openly accessible GNSS stations in the fast-subsiding area apparent from InSAR near the west end of the city (Figure 2). As illustrated by Lagos (Figure 2), the absence of GNSS data is even more pronounced for cities in many less-developed nations. Although InSAR data indicate that a large portion of the coastal area of Lagos is subsiding more rapidly than sea level is rising, there are no openly accessible GNSS data for any apparently subsiding locations in this region (Figure 2). In cities where openly accessible GNSS data are not available, true subsidence rates may be even higher than we have estimated from InSAR data, if the reference area is subsiding. As shown by these examples, InSAR results can provide a guide for where GNSS stations should be installed to more precisely monitor future subsidence.

The 2015–2020 InSAR results indicate that even in cities that are broadly stable, parts of the cities are sinking faster than sea level is rising. Many of these cities are so economically and/or culturally important that future coastal inundation will significantly impact both monetary values and human lives. We illustrate the global nature of this problem with the following examples:

1. Istanbul is the capital of Turkey with a population of 15 million. It is the largest city in Turkey and the most populous city in Europe. Although most of the city appears to be stable, an area of 5 × 20 km on the west end of the city is sinking faster than 2 mm/yr LOS
2. Lagos is the capital city of Nigeria. With a population of over 24 million, it is the most populous metropolitan area in Africa. An area of 5 × 10 km in the center of Lagos is subsiding faster than 2 mm/yr LOS
3. Taipei is the capital of Taiwan. It is the largest city in Taiwan, with a population of 2.7 million. It is in a basin on the north end of the island. Most of the city shows subsidence of more than 2 mm/yr LOS
4. Mumbai is the second-most populous city in India after Delhi. It is the seventh-most populous city in the world with a population of roughly 20 million. A significant portion of the city is subsiding more rapidly than 2 mm/yr LOS
5. Auckland is the largest city in New Zealand, with a population of 1.6 million. A significant portion of the area is subsiding more rapidly than 2 mm/yr LOS and the estimated low-elevation, fast-subsiding area is over 80 km²
6. The Tampa Bay Area surrounds Tampa Bay on the west coast of Florida (United States). It includes the cities of Tampa, St. Petersburg, and Clearwater. It is the eighteenth largest metropolitan area in the United States, with a population of over 3 million. A large area on the northwest side of the Tampa Bay area, including a 25-km-long section along the coast, is subsiding faster than 2 mm/yr LOS. The estimated area of this low-elevation, fast-subsiding portion of the Tampa metropolitan area is close to 800 km²

The cities with fastest subsidence rates are mostly in Asia. Jakarta is well known for its recent history of fast subsidence (Abidin et al., 2011). However, our InSAR results show that many more cities in South, South-east, and East Asia are characterized by areas of very fast subsidence. Figure 3 shows four populous cities with fast subsidence: Chittagong (Bangladesh), Tianjin (China), Manila (Philippines), and Karachi (Pakistan). The combined population of these four cities is 59 million. The maximum subsidence rate in Tianjin exceeds 40 mm/yr LOS (almost 20x mean sea level rise), in Chittagong and Manila exceeds 20 mm/yr LOS (almost 10x mean sea

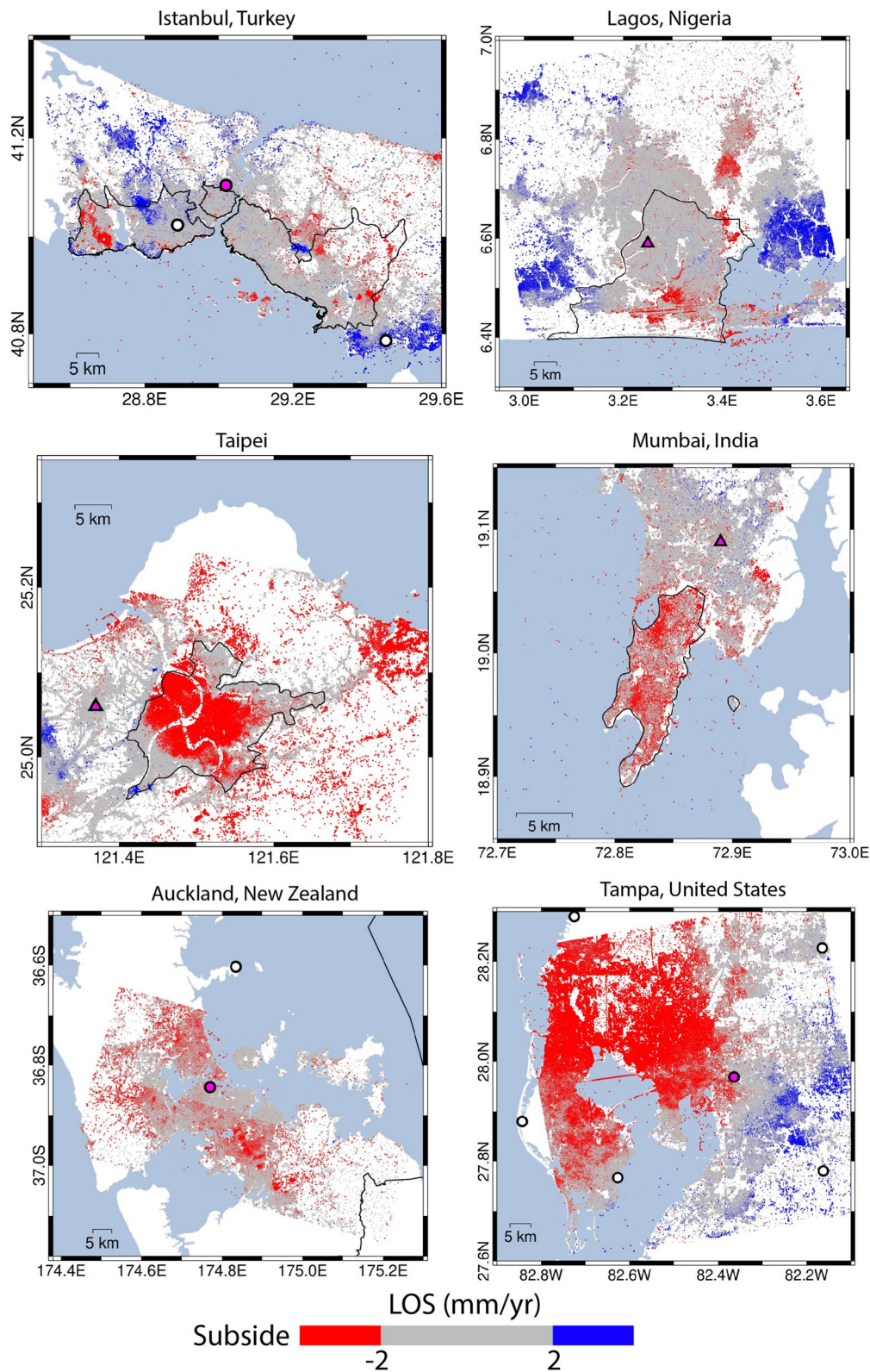
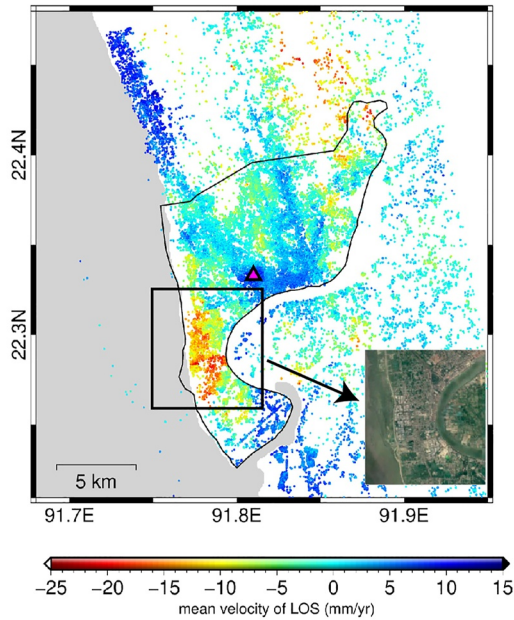
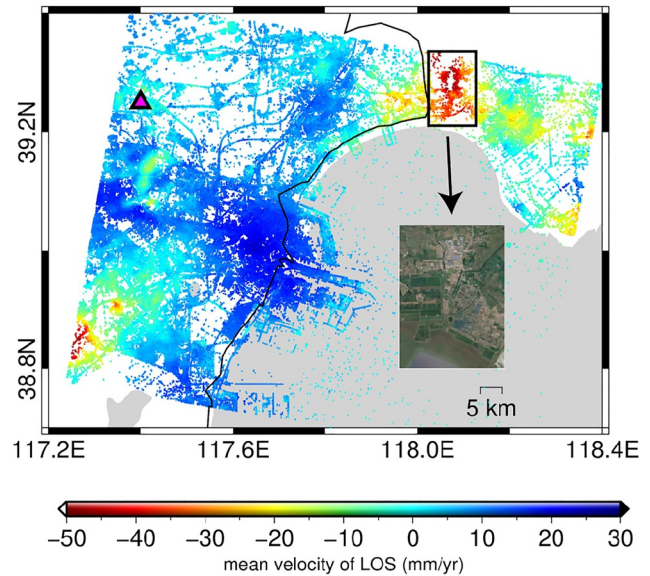


Figure 2. Mean line-of-sight (LOS) velocity distributions for selected cities. LOS velocities are in mm/yr between 2015 and 2020 using Sentinel-1 A/B data. Negative sign means the ground is moving away from the satellite, equivalent to subsidence in most cases. Circles are recent continuous Global Navigation Satellite System (GNSS) stations in the Nevada Geodetic Lab database. Magenta circles mark locations of reference stations used to shift the Interferometric Synthetic Aperture Radar (InSAR) data. Magenta triangles mark locations of 5-km radius circular areas used to shift the InSAR data in the absence of GNSS data.

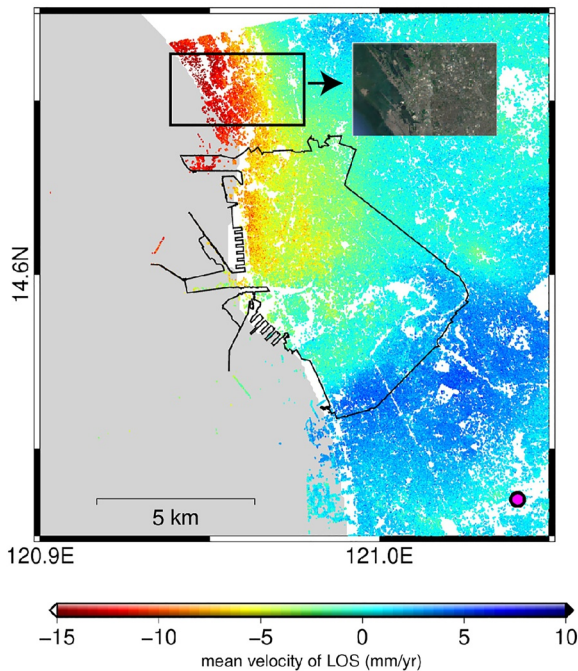
Chittagong, Bangladesh (9 million population)
Major financial center, Port city



Tianjin, China (12 million population)
Major port city in northern China



Manila, Philippines (22 million population)
Capital of Philippines, 2nd most populous city



Karachi, Pakistan (16 million population)
Capital of Pakistan

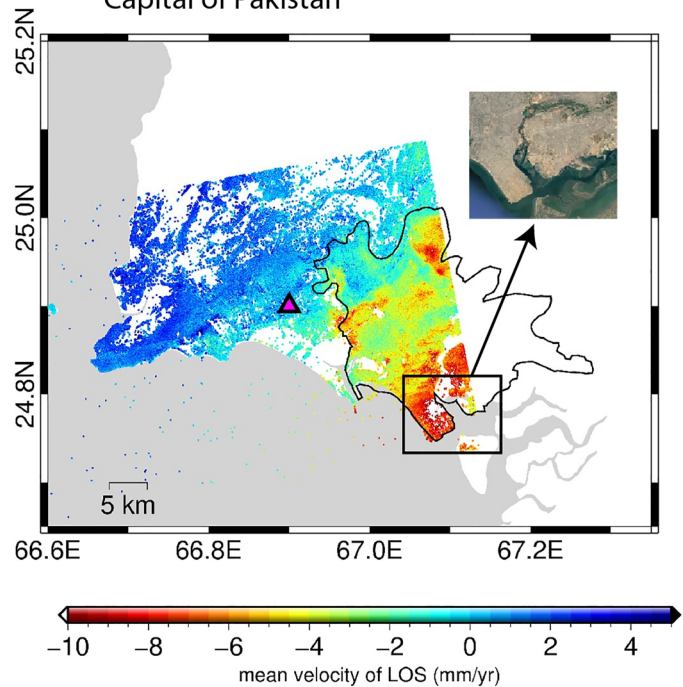


Figure 3. Selected coastal cities with significant subsidence (>10 mm/yr). Each black-outlined box shows the approximate area of the small inset, which is a screenshot from Google Earth. Magenta triangles mark locations of the 5-km radius circular areas used to shift the Interferometric Synthetic Aperture Radar data in the absence of Global Navigation Satellite System (GNSS) data. Magenta circles mark locations of reference GNSS stations. All the subsiding areas are residential or industrial, pointing to excessive groundwater extraction as the possible cause of subsidence.

level rise), and in Karachi exceeds 10 mm/yr (approximately 5x mean sea level rise). All the fast-subsiding areas shown in Figure 3 are either residential or industrial, suggesting that the subsidence is likely related to excessive groundwater extraction.

As these examples demonstrate, InSAR can be used to identify fast-subsiding areas. Because GNSS stations with openly accessible data are absent from the fast-sinking areas of these cities, the existence, extent, and rate of their subsidence would not be known without InSAR data.

3.2. Slowed Subsidence in Selected Cities

Fast subsidence has been previously reported for the Asian megacities of Jakarta and Shanghai. The subsidence rate exceeded 280 mm/yr in Jakarta between 1982 and 2010 (Abidin et al., 2011) and 16 mm/yr in Shanghai between 1990 and 2001 (Chai et al., 2004). Our 2015–2020 InSAR results indicate that subsidence rates in Jakarta and Shanghai have slowed significantly (Figure 4), likely due to reduced groundwater extraction rates implemented as government regulations (Yan et al., 2020). This slowing of subsidence by thoughtful groundwater management is not new. For example, subsidence was halted or slowed in Houston in the 1970s and Silicon Valley in the 1960s after organized remedial action (Ingebritsen & Galloway, 2014). These examples show that regulation can be an effective tool for stopping subsidence in areas where groundwater extraction is the main cause.

Despite this slowing of subsidence rates, our data show there are still areas of fast subsidence in these Asian megacities. In Jakarta, an area on the northwest coast of the city experiences subsidence of up to 20 mm/yr LOS. Also, Bekasi Regency, a suburb of Jakarta has been characterized by subsidence of up to 50 mm/yr LOS in recent years. This rapid subsidence in Bekasi Regency is likely due to groundwater extraction. The population of Bekasi Regency has grown from 2.6 million in 2010 to 3.1 million in 2020 (circa 20% increase over 10 years). Similar to Jakarta, most of Shanghai is stable, but many places near the water show subsidence up to 10 mm/yr LOS. Shanghai has the largest area of low-elevation, fast-subsidence of 1700 km².

3.3. Subsidence Mechanisms

As mentioned in the introduction, processes that affect coastal vertical motions include GIA and non-GIA components, with the latter including tectonic activity and sediment compaction (Hamlington et al., 2020). InSAR time series work best to capture regional subsidence caused by anthropogenic activities. Figure 5 shows examples from Semarang (Indonesia), Tampa (Florida, USA), and Tianjin (China).

In Semarang, subsidence of 20–30 mm/yr LOS characterizes a large portion of the city (Figure 5a). The geologic map of this region (Figure 5b) clearly shows that the subsiding area is alluvium, which is loose, unconsolidated soil, or sediment that has been eroded, reshaped by water in some form, and redeposited in a nonmarine setting. In contrast, the non-subsiding area is the Damar Formation, which is composed of tuffaceous sandstone, conglomerate, and volcanic breccia. The subsiding area includes both residential and industrial areas (Figure 5b). Given this lithologic difference, the subsidence in Semarang is likely caused by water extraction.

In Tampa, subsidence of up to 6 mm/yr LOS is observed in a large area north of Tampa Bay (Figure 5c). The subsiding area contains groundwater aquifers that are sources of freshwater for the cities (Figure 5d), suggesting that groundwater extraction contributes to the subsidence. The geological map of this region shows that the subsiding area is Pleistocene/Holocene sediment (Hutchinson, 1983). According to the official website, Tampa Bay Water is permitted to withdraw 120 million gallons per day from 13 wellfields in this area. Although Tampa Bay Water carefully monitors the environment in and around these wellfields, the subsidence of a few mm/yr apparent from InSAR could be overlooked due to the lack of an appropriate geodetic monitoring component.

In Tianjin, subsidence of 50 mm/yr LOS is observed on the northeast corner just outside of the city (Figure 5e). The area is centered in an industrial region with many factories (Figure 5f), which belongs to the city of Tangshan. This area is crossed by two small rivers and was farmland before 2013. Industrial groundwater extraction from subsurface alluvium may be the cause of subsidence in this area, as in Semarang.

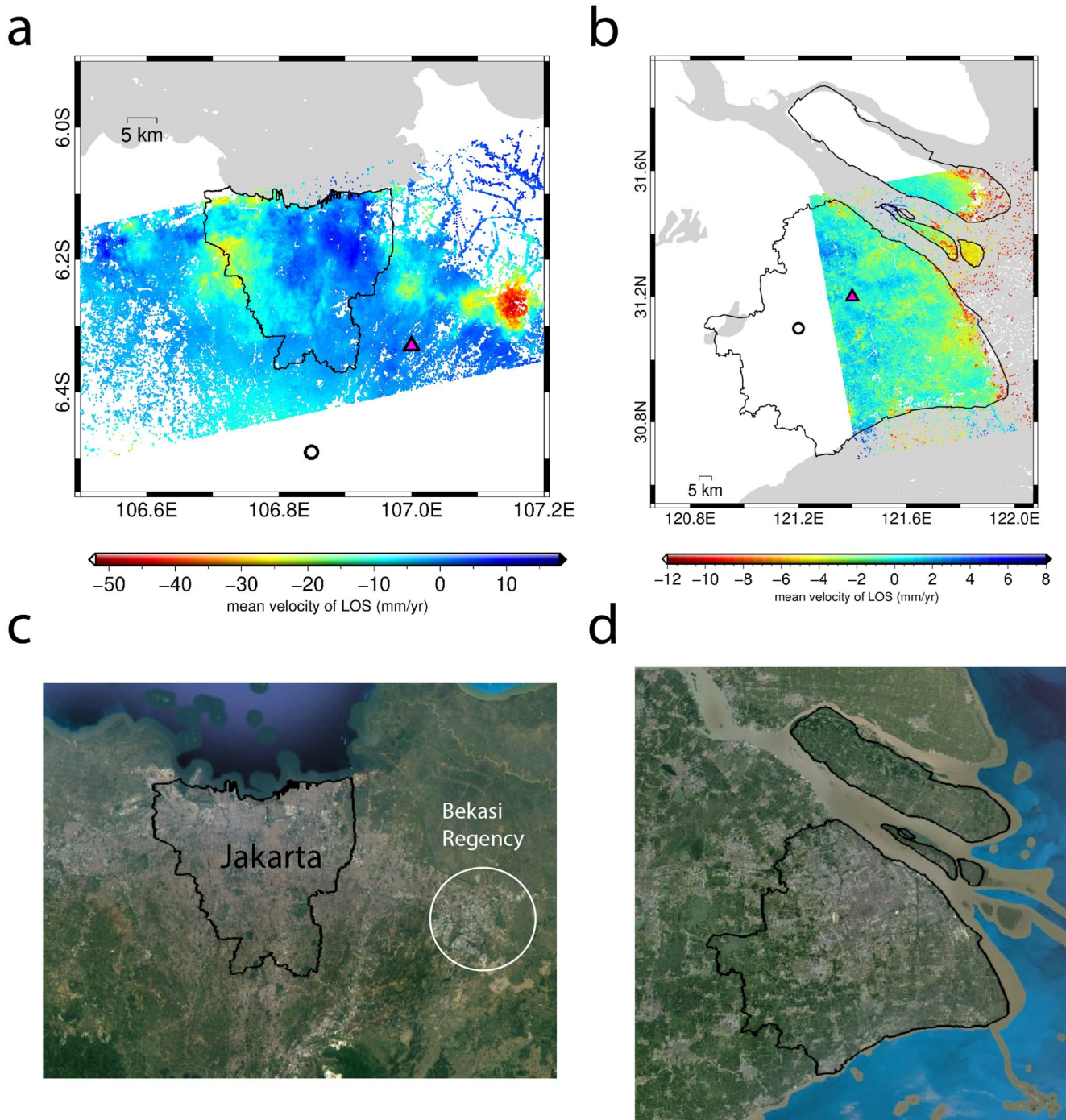


Figure 4. (a), (b) Subsidence maps of Jakarta and Shanghai. Black stroke circles are recent continuous Global Navigation Satellite System (GNSS) stations in the Nevada Geodetic Lab database (c), (d) Google Earth images of Jakarta and Shanghai. The black solid lines in all four panels mark the city boundaries. Magenta triangles mark locations of 5-km radius circular areas used to shift the Interferometric Synthetic Aperture Radar data in the absence of GNSS data.

4. Summary

InSAR results indicate that land is subsiding faster than sea level is rising in portions of many coastal cities throughout the world. This global problem largely results from local human action—especially groundwater withdrawal—in each city. The most rapid subsidence is occurring in South, Southeast, and East Asia, where population and water demand will continue to grow. Even in developed countries of North America, Europe,

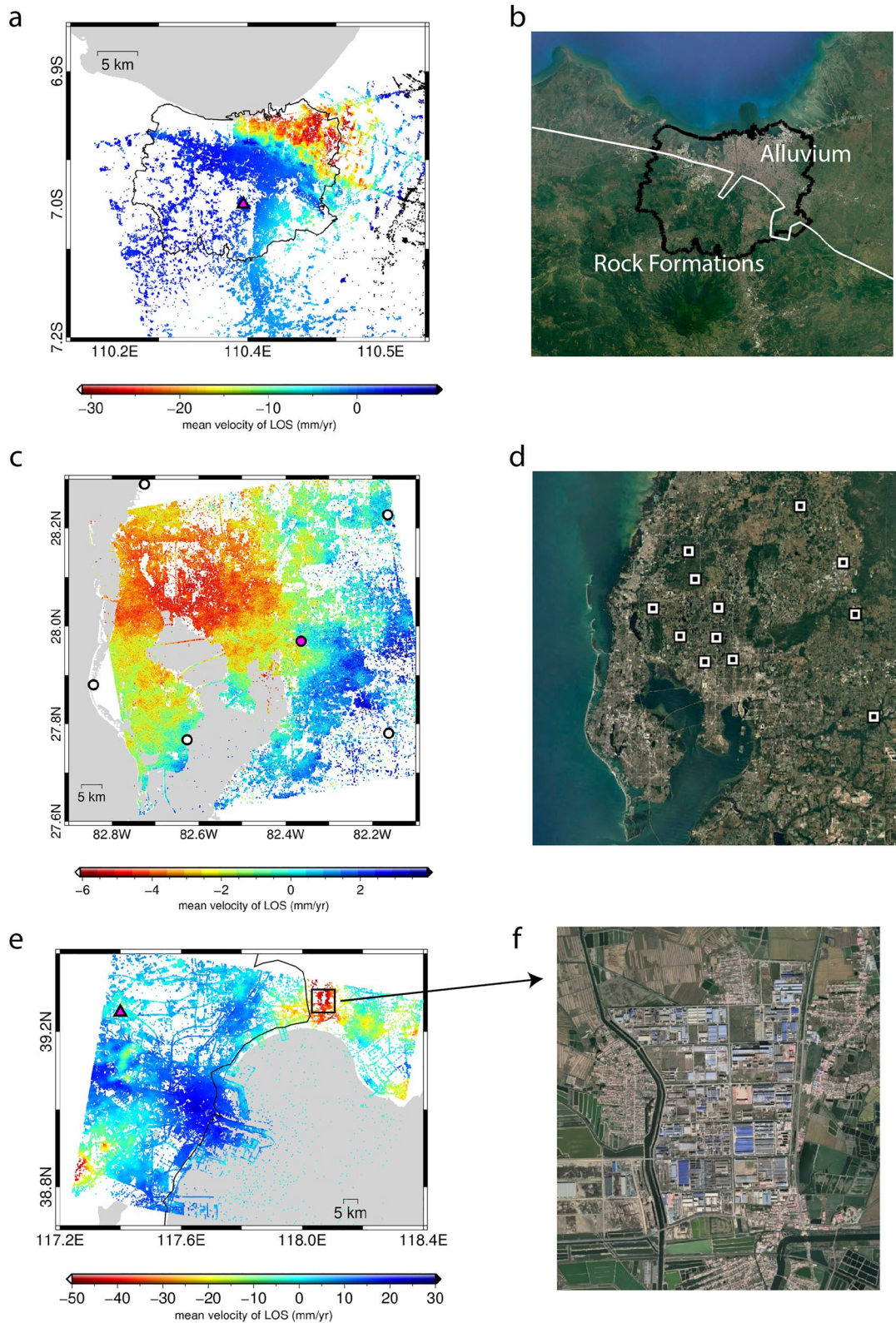


Figure 5. (a) Line-of-sight (LOS) velocity map of Semarang, Indonesia. The black solid line is the city boundary. (b) Google Earth image of Semarang. The solid black line is the city boundary. The white solid line is the boundary between Alluvium and rock formations. (c) LOS velocity map of Tampa, U. S. (d) Google Earth image of Tampa. The white squares are wellfields that extract underground water. (e) LOS velocity map of Tianjin, China. The solid black line is the city boundary. The black rectangle is the area of figure (f). (f) Google Earth image of the fast-sinking area on the top right in figure (e). The circles and triangles in (a, c, e) have the same meanings as in previous figures.

and Australia, parts of many cities appear to be sinking faster than sea level is rising. Continuous monitoring and policy intervention are required to reduce subsidence rates and minimize their consequences. Known examples of sustained and reasonably successful management of coastal subsidence involve relatively localized subsidence, effective governance, and large capital investment (Ingebritsen & Galloway, 2014). It will be a challenge to reproduce this success in cities throughout the world. However, cities and nations that fail to address the cause(s) of their subsidence will be challenged by flooding much sooner than projected by sea level rise models.

Data Availability Statement

InSAR data used in this research can be downloaded freely online from the Copernicus Open Access Hub from ESA (<https://scihub.copernicus.eu/>) or the Alaska SAR Facility (<https://asf.alaska.edu/>). To download, just search Sentinel-1 data for your area of interest and time window. The processing software SNAP (<https://step.esa.int/main/download/snap-download/>) and StaMPS (<https://github.com/dbekaert/StaMPS>) are also available online. Shuttle Radar Topography Mission elevation data can be downloaded freely from USGS data center (<https://lpdaac.usgs.gov/>). To download, select your area of interest. Under the data sets tab, select Digital Elevation > SRTM > SRTM 1-ArcSecond Global. InSAR LOS displacement rate map for all the cities can be downloaded at <https://doi.org/10.5281/zenodo.5635199>.

Acknowledgments

P. W. is supported by a Government Fellowship from Taiwan.

References

- Abidin, H. Z., Andreas, H., Gumilar, I., Fukuda, Y., Pohan, Y. E., & Deguchi, T. (2011). Land subsidence of Jakarta (Indonesia) and its relation with urban development. *Natural Hazards*, 59(3), 1753–1771. <https://doi.org/10.1007/s11069-011-9866-9>
- Bekaert, D. P. S., Walters, R. J., Wright, T. J., Hooper, A. J., & Parker, D. J. (2015). Statistical comparison of InSAR tropospheric correction techniques. *Remote Sensing of Environment*, 170, 40–47. <https://doi.org/10.1016/j.rse.2015.08.035>
- Blackwell, E., Shirzaei, M., Ojha, C., & Werth, S. (2020). Tracking California's sinking coast from space: Implications for relative sea-level rise. *Science Advances*, 6(31), 1–10. <https://doi.org/10.1126/sciadv.aba4551>
- Cao, A., Esteban, M., Valenzuela, V. P. B., Onuki, M., Takagi, H., Thao, N. D., & Tsuchiya, N. (2021). Future of Asian Deltaic Megacities under sea level rise and land subsidence: Current adaptation pathways for Tokyo, Jakarta, Manila, and Ho Chi Minh City. *Current Opinion in Environmental Sustainability*, 50, 87–97. <https://doi.org/10.1016/j.cosust.2021.02.010>
- Chai, J. C., Shen, S. L., Zhu, H. H., & Zhang, X. L. (2004). Land subsidence due to groundwater drawdown in Shanghai. *Géotechnique*, 54(2), 143–147. <https://doi.org/10.1680/geot.2004.54.2.143>
- Chaussard, E., Amelung, F., Abidin, H., & Hong, S. H. (2013). Sinking cities in Indonesia: ALOS PALSAR detects rapid subsidence due to groundwater and gas extraction. *Remote Sensing of Environment*, 128, 150–161. <https://doi.org/10.1016/j.rse.2012.10.015>
- Ciampalini, A., Solari, L., Giannecchini, R., Galanti, Y., & Moretti, S. (2019). Evaluation of subsidence induced by long-lasting buildings load using InSAR technique and geotechnical data: The case study of a Freight Terminal (Tuscany, Italy). *International Journal of Applied Earth Observation and Geoinformation*, 82, 101925. <https://doi.org/10.1016/j.jag.2019.101925>
- Collados-Lara, A. J., Pulido-Velazquez, D., Mateos, R. M., & Ezquerro, P. (2020). Potential impacts of future climate change scenarios on ground subsidence. *Water (Switzerland)*, 12(1), 219. <https://doi.org/10.3390/w12010219>
- Dixon, T. H., Amelung, F., Ferretti, A., Novali, F., Rocca, F., Dokka, R., et al. (2006). Subsidence and flooding in New Orleans. *Nature*, 441(7093), 587–588. <https://doi.org/10.1038/441587a>
- Dokka, R. K. (2006). Modern-day tectonic subsidence in coastal Louisiana. *Geology*, 34(4), 281–284. <https://doi.org/10.1130/g22264.1>
- Erkens, G., Bucx, T., Dam, R., De Lange, G., & Lambert, J. (2015). Sinking coastal cities. *Proceedings of the International Association of Hydrological Sciences*, 372, 189–198. <https://doi.org/10.5194/piahs-372-189-2015>
- Esteban, M., Takagi, H., Nicholls, R. J., Fatma, D., Pratama, M. B., Kurobe, S., et al. (2020). Adapting ports to sea-level rise: Empirical lessons based on land subsidence in Indonesia and Japan. *Maritime Policy & Management*, 47(7), 937–952. <https://doi.org/10.1080/03088839.2019.1634845>
- Farolfi, G., Bianchini, S., & Casagli, N. (2019). Integration of GNSS and satellite InSAR data: Derivation of fine-scale vertical surface motion maps of Po plain, northern Apennines, and southern Alps, Italy. *IEEE Transactions on Geoscience and Remote Sensing*, 57(1), 319–328. <https://doi.org/10.1109/tgrs.2018.2854371>
- Fielding, E. J., Blom, R. G., & Goldstein, R. M. (1998). Rapid subsidence over oil fields measured by SAR interferometry. *Geophysical Research Letters*, 25(17), 3215–3218. <https://doi.org/10.1029/98gl52260>
- Fritz, H. M., Blount, C., Sokoloski, R., Singleton, J., Fuggle, A., McAdoo, B. G., et al. (2007). Hurricane Katrina storm surge distribution and field observations on the Mississippi Barrier Islands. *Estuarine, Coastal and Shelf Science*, 74(1–2), 12–20. <https://doi.org/10.1016/j.ecss.2007.03.015>
- Galloway, D. L., Jones, D. R., & Ingebritsen, S. E. (Eds.), (1999). *Land subsidence in the United States (vol. 1182)*. US Geological Survey. <https://doi.org/10.3133/cir1182>
- Garner, A. J., Mann, M. E., Emanuel, K. A., Kopp, R. E., Lin, N., Alley, R. B., et al. (2017). Impact of climate change on New York City's coastal flood hazard: Increasing flood heights from the preindustrial to 2300 CE. *Proceedings of the National Academy of Sciences of the United States of America*, 114(45), 11861–11866. <https://doi.org/10.1073/pnas.1703568114>
- Hamlington, B. D., Gardner, A. S., Ivins, E., Lenaerts, J. T. M., Reager, J. T., Trossman, D. S., et al. (2020). Understanding of Contemporary regional sea-level change and the implications for the future. *Reviews of Geophysics*, 58(3), 1–39. <https://doi.org/10.1029/2019RG000672>
- Hammond, W. C., Burgette, R. J., Johnson, K. M., & Blewitt, G. (2018). Uplift of the Western transverse ranges and Ventura area of Southern California: A four-technique geodetic study combining GPS, InSAR, leveling, and tide gauges. *Journal of Geophysical Research: Solid Earth*, 123(1), 836–858. <https://doi.org/10.1002/2017jb014499>

- He, Y., Xu, G., Kaufmann, H., Wang, J., Ma, H., & Liu, T. (2021). Integration of InSAR and LiDAR technologies for a detailed urban subsidence and hazard assessment in Shenzhen, China. *Remote Sensing*, *13*(12), 2366. <https://doi.org/10.3390/rs13122366>
- Herrera-García, G., Ezquerro, P., Tomás, R., Béjar-Pizarro, M., López-Vinielles, J., Rossi, M., et al. (2021). Mapping the global threat of land subsidence. *Science*, *371*(6524), 34–36. <https://doi.org/10.1126/science.abb8549>
- Hooper, A., Zebker, H., Segall, P., & Kampes, B. (2004). A new method for measuring deformation on volcanoes and other natural terrains using InSAR persistent scatterers. *Geophysical Research Letters*, *31*(23). <https://doi.org/10.1029/2004gl021737>
- Hu, B., Chen, J., & Zhang, X. (2019). Monitoring the land subsidence area in a coastal urban area with InSAR and GNSS. *Sensors*, *19*(14), 3181. <https://doi.org/10.3390/s19143181>
- Hung, W. C., Hwang, C., Chen, Y. A., Zhang, L., Chen, K. H., Wei, S. H., et al. (2018). Land subsidence in Chiayi, Taiwan, from compaction well, leveling and alos/palsar: Aquaculture-induced relative sea level rise. *Remote Sensing*, *10*(1), 40.
- Hutchinson, C. B. (1983). *Assessment of the interconnection between Tampa Bay and the Floridan Aquifer*. Geological Survey Tallahassee Florida Water Resources Div.
- Ingebritsen, S. E., & Galloway, D. L. (2014). Coastal subsidence and relative sea level rise. *Environmental Research Letters*, *9*(9), 091002. <https://doi.org/10.1088/1748-9326/9/9/091002>
- Karegar, M. A., Dixon, T. H., Malservisi, R., Kusche, J., & Engelhart, S. E. (2017). Nuisance flooding and relative sea-level rise: The importance of present-day land motion. *Scientific Reports*, *7*(1), 1–9. <https://doi.org/10.1038/s41598-017-11544-y>
- Kulp, S. A., & Strauss, B. H. (2019). New elevation data triple estimates of global vulnerability to sea-level rise and coastal flooding. *Nature Communications*, *10*(1). <https://doi.org/10.1038/s41467-019-12808-z>
- Métouis, M., Benjelloun, M., Lasserre, C., Grandin, R., Barrier, L., Dushi, E., & Koçi, R. (2020). Subsidence associated with oil extraction, measured from time series analysis of Sentinel-1 data: Case study of the Patos-Marinza oil field, Albania. *Solid Earth*, *11*(2), 363–378.
- Morishita, Y. (2021). Nationwide urban ground deformation monitoring in Japan using Sentinel-1 LiCSAR products and LiCSBAS. *Progress in Earth and Planetary Science*, *8*(1), 1–23. <https://doi.org/10.1186/s40645-020-00402-7>
- Nicholls, R. J., Lincke, D., Hinkel, J., Brown, S., Vafeidis, A. T., Meyssignac, B., et al. (2021). A global analysis of subsidence, relative sea-level change and coastal flood exposure. *Nature Climate Change*, *11*, 338–342. <https://doi.org/10.1038/s41558-021-00993-z>
- Osmanoğlu, B., Sunar, F., Wdowski, S., & Cabral-Cano, E. (2016). Time series analysis of InSAR data: Methods and trends. *ISPRS Journal of Photogrammetry and Remote Sensing*, *115*, 90–102. <https://doi.org/10.1016/j.isprsjprs.2015.10.003>
- Palmer, M. D., Domingues, C. M., Slangen, A. B. A., & Boeira Dias, F. (2021). An ensemble approach to quantify global mean sea-level rise over the 20th century from tide gauge reconstructions. *Environmental Research Letters*, *16*(4). <https://doi.org/10.1088/1748-9326/abdacc>
- Sato, C., Haga, M., & Nishino, J. (2006). Land subsidence and groundwater management in Tokyo. *International Review for Environmental Strategies*, *6*(2), 403–424.
- Shirzaei, M., & Bürgmann, R. (2018). Global climate change and local land subsidence exacerbate inundation risk to the San Francisco Bay Area. *Science Advances*, *4*(3), eaap9234. <https://doi.org/10.1126/sciadv.aap9234>
- Shirzaei, M., Freymueller, J., Törnqvist, T. E., Galloway, D. L., Dura, T., & Minderhoud, P. S. J. (2021). Measuring, modelling and projecting coastal land subsidence. *Nature Reviews Earth & Environment*, *2*(1), 40–58. <https://doi.org/10.1038/s43017-020-00115-x>
- Smith-Konter, B. R., Thornton, G. M., & Sandwell, D. T. (2014). Vertical crustal displacement due to interseismic deformation along the San Andreas fault: Constraints from tide gauges. *Geophysical Research Letters*, *41*(11), 3793–3801.
- Teatini, P., Tosi, L., Strozzi, T., Carbognin, L., Wegmüller, U., & Rizzetto, F. (2005). Mapping regional land displacements in the Venice coastland by an integrated monitoring system. *Remote Sensing of Environment*, *98*(4), 403–413. <https://doi.org/10.1016/j.rse.2005.08.002>
- Ward, P. J., Marfai, M. A., Yulianto, F., Hizbaron, D. R., & Aerts, J. C. J. H. (2011). Coastal inundation and damage exposure estimation: A case study for Jakarta. *Natural Hazards*, *56*(3), 899–916. <https://doi.org/10.1007/s11069-010-9599-1>
- Yalvac, S. (2020). Validating InSAR-SBAS results by means of different GNSS analysis techniques in medium-and high-grade deformation areas. *Environmental Monitoring and Assessment*, *192*(2), 1–12. <https://doi.org/10.1007/s10661-019-8009-8>
- Yan, X., Yang, T., Yan, X. U., Tosi, L., Stouthamer, E., Andreas, H., et al. (2020). Advances and practices on the research, prevention and Control of land subsidence in coastal cities. *Acta Geologica Sinica*, *94*(1), 162–175. <https://doi.org/10.1111/1755-6724.14403>